Geoderma 430 (2023) 116286

Contents lists available at ScienceDirect

Geoderma

journal homepage: www.elsevier.com/locate/geoderma

Iron isotope fractionation during the formation of ferromanganese nodules under different conditions of hydromorphism

Péter Sipos [a,b,*], Ivett Kovács [a,b], Gyöngyi Barna [c], Adrienn Tóth [b,d], András Makó [c], László Palcsu [e], Gabriella Kiss [e], Anikó Horváth [e], Anita Puskás-Preszner [e]

[a] Institute for Geological and Geochemical Research, Research Centre for Astronomy and Earth Sciences, Eötvös Loránd Research Network, H1112 Budapest, Budaörsi út 45, Hungary
[b] CSFK, MTA Centre of Excellence, Konkoly-Thege Miklós út 15-17, Budapest H-1121, Hungary
[c] Institute for Soil Sciences, Centre for Agricultural Research, Eötvös Loránd Research Network, Herman Ottó út 15, H1022 Budapest, Hungary
[d] Geographical Institute, Research Centre for Astronomy and Earth Sciences, Eötvös Loránd Research Network, Budaörsi út 45, H1112 Budapest, Hungary
[e] Isotope Climatology and Environmental Research Centre, Institute for Nuclear Research, Eötvös Loránd Research Network, Bem tér 18/C, H4026 Debrecen, Hungary

ARTICLE INFO

Handling Editor: Daniel Said-Pullicino

Keywords:
Fe isotopes
Hydromorphic soils
Ferromanganese nodules
Redox processes

ABSTRACT

Hydromorphic soils are often characterized by redoximorphic pedofeatures like ferromanganese nodules. As the highly varying properties of the nodules are sensitive indicators of the pedogenic processes and redox history of the soil, their isotopic study may get a deeper insight into the soil genesis. In this study, the Fe isotopic characteristics, fabric, and mineralogy of ferromanganese nodules formed in six hydromorphic soil profiles were investigated using MC-ICP-MS, EPMA, and XRD analyses. We aimed to relate the Fe isotopic composition of the bulk soils and nodules to the varying conditions of hydromorphism and the various properties of the nodules.

Although the extent of hydromorphism could be related to the nodules' properties, such a relationship was not found with their Fe isotopic characteristics. The reductive dissolution of primary Fe minerals resulted in similar Fe isotope distribution characteristics for the bulk soils. However, specific features of hydromorphic conditions (like frequency of the redox cycles, relocation of water fluctuation zone, external Fe input, and inhibition of leaching) affected the Fe isotope characteristics of both bulk soils and nodules. The minimum δ^{56}Fe value within the soil profile indicated the deepest part where precipitation of light Fe may dominate over its leaching. Above this depth, the isotopically light Fe precipitated to form the nodules. However, the higher frequency of the reductive conditions was responsible for the higher mobilization of isotopically light Fe below this depth. The isotopic characteristics of the nodules supported that authigenic Fe-oxyhydroxides were enriched in the light Fe isotope.

The Fe isotope composition of a given soil horizon and its nodules result from a complex interaction of different processes whose effect varies from profile to profile. The integrated study of the Fe isotope characteristics of hydromorphic soils and their nodules may help follow several pedogenic processes and conditions.

1. Introduction

Hydromorphic soils are characterized by the reduction or localized segregation of iron, owing to the temporary or permanent waterlogging of the soil pores, causing the lack of oxygen over a relatively long period. The reductive dissolution of primary iron minerals results in the mobilization, translocation, and subsequent oxidation of iron leading to the formation of redoximorphic features in the soil. In addition, periodic fluctuations in groundwater levels have been shown to affect wet and dry conditions and Eh values in the soil, which may trigger the formation of ferromanganese nodules (Stiles et al., 2001). These formations can be characterized by a largely variable external habit, fabric, chemistry, and mineralogy. These features reflect sensitively the pedogenic environment and redox history of the soil in which they have formed (Gasparatos et al., 2019).

Dynamic changes in the valence state of iron in response to varying redox conditions affect several processes, like mineral weathering, nutrient cycling, contaminant mobility (Cornell and Schwertmann,

* Corresponding author at: Institute for Geological and Geochemical Research, Research Centre for Astronomy and Earth Sciences, Eötvös Loránd Research Network, H1112 Budapest, Budaörsi út 45, Hungary.
E-mail address: sipos.peter@csfk.org (P. Sipos).

https://doi.org/10.1016/j.geoderma.2022.116286
Received 14 July 2022; Received in revised form 27 October 2022; Accepted 22 November 2022
Available online 1 December 2022

2003), and even the preservation of organic carbon (Kaiser and Guggenberger, 2000). Therefore, the detailed study of the dynamics of iron phases is a critical issue in hydromorphic soils. The iron isotopic composition of redoximorphic soils is a sensitive indicator of the changes in iron dynamics. The fractionation of iron isotopes in soils can be the result of abiotic processes (dissolution, adsorption, precipitation, mineral transformation), biotic processes (microbial reduction and oxidation), and a combination of both pathways resulting in the preferential release of the light Fe isotope to the soil solution (Johnson et al., 2002).

In soils with groundwater-induced redoximorphosis, several studies showed the isotopically lighter character of iron in the Fe-enrichment zones. Differences in the isotopic composition between the organic and mineral horizons were explained by the differences in the immobilization processes (precipitation vs adsorption) of the iron (Mansfeldt et al., 2012) or by the increasing effect of the parent materials' Si-bound iron downwards (Fekiacova et al., 2013). Additionally, Schuth and Mansfeldt (2016) observed strongly varying iron isotope composition of the soil solution with the abundance of iron oxyhydroxides suggesting that groundwater fluctuation affects both aqueous and mineral iron in the soil. Huang et al. (2018) observed similar distribution characteristics for the iron isotope composition in paddy soils. According to Garnier et al. (2017), the isotope fractionation between the pore water and the soil involved three iron pools in such soils such as Fe(II) in solution, adsorbed Fe(II), and reactive Fe(III) in the (mineral) phases. In Gleysols, significant iron isotope fractionation was observed between the Fe-enriched and depleted parts even within soil horizons despite the very small or no Fe isotope fractionation at the profile scale (Wiederhold et al., 2007; Fekiacova et al., 2021). In addition, the isotopically lighter character of paleo-mottles and nodules was found by Schulz et al. (2016) and Feng et al. (2018), respectively.

Despite the recent increase in studies, iron isotopic investigations of bulk soils are still limited. Additionally, such studies are still lacking in several soil types like Vertisols, Solonetz, Chernozems, etc. (Wu et al., 2019). Although several recent studies supported the mobilization of isotopically light iron under reductive dissolution in soils, the explanations are quite diverse due to the numerous processes and conditions present in soils. The ferromanganese nodules represent the redox dynamics of iron in soils spectacularly, and they may appear in various soil types. Thus, their isotopic study may get a deeper insight into soil genesis as the highly variable characteristics of the nodules are sensitive indicators of pedogenic processes. Moreover, isotopic studies have focused on paleo-nodules so far. This study intends to fill the above gaps through the iron isotopic study of soils and ferromanganese nodules formed under different conditions of hydromorphism. The primary aims were to reveal the differences in the isotopic compositions of the bulk soils and ferromanganese nodules and to relate these differences to the varying conditions of hydromorphism and the various properties of the nodules.

2. Materials and methods

2.1. Soils, nodules, and their preparation for the analyses

Six soil profiles were sampled by genetic horizons from soil pits. The sampling sites were located mostly on alluvial plains (Pellic Vertisol; Phaeozem) with loessal influence in several cases (Vertisol, Gleysol, Solonetz) on nearly level (Vertisol, Solonetz, Phaeozem) or very gentle slopes (Gleysol, Pellic Vertisol). The Luvisol profile was sampled at the transition area of a loessal hill and an alluvial plain on a moderate slope. The groundwater table was reached during the sampling of the Gleysol (at 110 cm) and the Phaeozem (at 120 cm) profiles only. The mean annual temperature was similar (between 9.5 and 10.0 °C) at the sampling sites, whereas the precipitation increased as follows: Vertisol and Solonetz (550 mm), Pellic Vertisol (600 mm), Phaeozem (640 mm), Gleysol (690 mm), and Luvisol (760 mm) (Dövényi, 2010).

The soil profiles were described according to the FAO guidelines (FAO, 2006), and the WRB system was used for classification (FAO, 2014). The sampled profiles represented different soil types formed under varying hydromorphic conditions characterized by shallow groundwater (Vertisol, Gleysol, and Solonetz), stagnant surface water (Pellic Vertisol and Luvisol), and temporal flooding (Phaeozem). The soil qualifiers and locations of the sampling sites are shown in Table 1. Before the physicochemical characterization of the soils, the samples were air-dried, gently crushed, and sieved through a 2 mm sieve. Then, the samples were crushed further to coarse (<100 μm) and fine (<10 μm) powder in an agate mortar for their mineralogical and chemical analyses, respectively.

Ferromanganese nodules appeared in the soil profiles at varying depth intervals (Table 1). They were separated from the soils according to Gasparatos et al. (2005). Briefly, 200 g of air-dried soil was dispersed in 500 ml of 0.25 M Na_2CO_3 overnight, then the > 1 mm fraction was wet-sieved and washed with distilled water. The nodules were manually separated from the oven-dried > 1 mm soil fraction under the stereomicroscope (Nikon SMZ800). Two grams of nodule separates were crushed for the mineralogical and chemical analyses as described for the soil samples. Further 4 to 6 nodules from each sample were selected for the electron microscopic studies. These nodules were set into epoxy resin using vacuum impregnation (Struers Citovac), and then the impregnated nodules were cut (Struers Minitom) to show a cross-section and micro-polished (Struers LaboPol-5). The polished surfaces were documented under the stereomicroscope and then coated with carbon for electron microscopic analyses (JEOL JFC 1200 fine coater).

2.2. Soils characterization

The soil pH was analyzed by the potentiometric method in a soil-distilled water suspension at a ratio of 1:2.5 (McLean, 1982). The soil organic matter content was determined by wet combustion using the Tyurin titrimetric method (Nelson and Sommers, 1996). The calcium carbonate content of the soils was studied by the Scheibler calcimeter (Nelson, 1982). The conventional sieve-pipette method was used to measure the particle-size distribution of the samples (Gee and Bauder, 1986).

The mineralogical composition of the bulk soils was analyzed by X-ray diffractometry at 40 kV and 15 mA using Cu Ka radiation (Rigaku Miniflex 600). The powdered material was loaded into steel holders to obtain random powder mounts. The 2θ range was set to 2-70°, and a counting speed of 0.05°/2 secs was used for the analyses. The Rigaku PDXL2 software was used for the phase identification based on the ICDD database. The total iron concentrations of the soil samples were analyzed by energy-dispersive X-ray fluorescent spectrometry (Spectro XSort Combi).

2.3. Nodules characterization

The mineralogical and chemical composition of the bulk nodules were analyzed as described for the soil samples. Additionally, the diffraction patterns were also processed using the Siroquant V4 software, and the phase compositions of the samples were determined by the Rietveld method.

The micro-fabric of the nodules was studied by electron probe microanalysis (JEOL Superprobe JCXA-733). An acceleration voltage of 20 kV and a probe current of 6nA were used for the analyses. The studied areas were documented using backscattered electron micrographs. The internal fabric of the nodules was described according to Stoops (2020).

2.4. Iron isotope analyses

Samples were digested using ammonium-bifluoride (NH_4HF_2; ABF) according to Újvári et al. (2021). Depending on the Fe concentrations in the samples, 12.6–202.5 mg of samples (equaling 5 mg/l Fe in the final

Table 1
The major physicochemical properties of the studied soils. *Goehtite detected by XRD in the bulk soil (BS) or clay farction (CF); ** Groundwtaer table was reached at 110 and 120 cm in the Gleysol and Phaeozem profiles, respectively. n.a. = not analysed.

	Depth (cm)	pH	SOM (%)	Calcium carbonate (%)	Silt (2–50 μm) (%)	Clay (<2μm) (%)	Fe %	Presence of goethite*	Nodule frequency
Soils with shallow groundwater									
Epigleyic Epistagnic Mollic Endocalcic VERTISOL/Kisújszállás (47.23564 N; 20.73574 E)									
A	0–25	6.80	2.1	0	38.2	44.6	4.38	n.d.	+
AB	25–55	7.60	1.3	0	42.8	45.0	4.97	CF	++
B	55–85	8.10	–	15.3	41.1	45.7	5.37	BS, CF	++
C	85–100	8.10	–	7.3	47.2	40.9	4.32	n.d.	–
Mollic Calcic GLEYSOL/Zalanszentlászló (46.89494 N; 17.10051E)									
A1	0–20	7.57	5.5	1.0	44.1	15.8	2.91	n.d.	–
A2	20–55	8.06	1.4	6.3	30.4	23.1	3.04	CF	+++
B	55–90	8.43	0.5	34.6	34.6	17.1	3.11	n.d.	–
C**	90-	n.a.	n.a.	n.a.	n.a.	n.a.	n.a.	n.a.	–
Vertic Endosalic Mollic Endogleyic Epistagnic SOLONETZ/Püspökladány (47.34989 N; 21.09302 E)									
A	0–5	6.32	3.7	0	39.8	28.5	2.80	n.d.	–
B1	5–30	6.77	1.8	0	35.2	41.1	4.09	n.d.	+
B2	30–80	8.02	1.0	0.5	32.4	50.5	4.69	n.d.	++
BC	80–130	9.14	0.4	4.0	36.3	44.2	4.63	n.d.	++
C	130–160	9.26	0.2	4.0	36.7	50.5	7.45	n.d.	–
Soils with stagnant surface water									
Pellic VERTISOL/Verpelét (47.86819 N; 20.20072 E)									
A1	0–30	6.18	2.6	0.08	40.2	45.4	3.70	n.d.	–
A2	30–65	6.51	1.7	0.04	36.6	51.1	3.97	n.d.	++
AB	65–90	7.06	1.3	0.08	37.1	52.3	4.03	n.d.	–
Endostagnic LUVISOL/Szentpéterfölde (46.60405 N; 16.74462 E)									
A	0–30	7.29	2.7	0.5	53.6	12.9	3.46	n.d.	–
B	30–50	7.50	1.2	0.6	54.0	16.8	3.81	n.d.	–
C1	50–67	7.42	0.5	0.1	51.0	29.9	4.53	BS, CF	++
*C*2	67–120	7.42	0.5	0.1	41.4	32.7	4.71	CF	++
C3	120–150	6.68	0.2	0.1	43.1	30.7	n.a.	n.d.	–
Soils with regular flooding									
Stagnic Fluvic PHAEOZEM/Rábapaty (47.31862 N; 16.96841 E)									
A1	0–15	7.89	3.0	0.4	11.2	36.3	5.19		–
A2	15–35	7.88	2.7	0.4	11.0	36.9	4.58	BS, CF	+
B	35–50	7.97	1.6	0.4	13.2	38.6	5.69	BS, CF	++
C1	50–75	7.95	1.0	0.5	12.0	35.7	6.05	BS, CF	++
*C*2	75–110	7.98	0.8	0.3	10.2	31.3	5.99	BS, CF	++
C3**	110-	n.a.	n.a.	n.a.	n.a.	n.a.	n.a.	n.a.	–

solution) were measured into PFA beakers with the ABF at the 5:1 ABF: sample mass ratio. The mixtures were heated to 230 °C for 24 h in a heating cabinet. After cooling down, 2 ml suprapur cc. (67 %) HNO_3 was added to the salt cakes and left on a hotplate for 1 h at 160 °C. These sample solutions were subsequently evaporated to dryness. After taking them up in 8 M HNO_3, samples were heated to 120 °C on a hotplate for 6 h. The final clear solutions were dried again, treated with 2 ml of suprapur 6 M HCl and 0.26 mM H_2O_2 for 1 h on a hotplate at 120 °C, and evaporated to dryness. Finally, they were taken up in 4 ml of 6 M HCl and 0.26 mM H_2O_2 before ion-exchange chromatography. Chemical separation was carried out following an adaptation of the procedure by de Jong et al. (2007). The iron content of the samples was separated from sample matrix constituents using Bio-Rad AG-MP1 (100–200 mesh) strong anionic exchange resin.

A Thermo Scientific Neptune Plus MC-ICP-MS instrument was used for Fe isotope ratio measurements in wet plasma operation. The isotope ratio measurements were carried out at high mass resolution on the interference-free left plateau of the peak, thus avoiding spectral interference. Two isotopic ratios were measured ($^{56}Fe/^{54}Fe$, and $^{57}Fe/^{54}Fe$) by a combination of standard-sample bracketing and external normalization. Data were reported in delta (δ) notation in permil (‰) relative to the international Fe standard IRMM-524B calculated as.

$$\delta^{5x}Fe = \left(\frac{^{5x}Fe/^{54}Fe_{sample}}{^{5x}Fe/^{54}Fe_{IRMM524B}} - 1\right) \times 1000$$where × stands for 6 or 7. In a $\delta^{57}Fe$ vs $\delta^{56}Fe$ plot, all data could be found along a line with a slope equaling the theoretical value of ln (M57/M54)/ln(M56/M54) = 1.48 (Craddock and Dauphas, 2011), indicating mass-dependent fractionation and no influence of isobaric interferences.

3. Results

3.1. Soils characteristics

The major physicochemical properties of the studied soils are shown in Table 1. The soil pH values varied over a wide range. They mostly fell in the alkaline range except for the Luvisol, which showed neutral pH through the profile. The topsoil samples sometimes showed neutral (Vertisol) or even acidic (Solonetz, Pellic Vertisol) character, and the subsoil of the Solonetz profile was strongly alkaline. The organic matter content of the soils did not show extreme concentrations, with the highest value (5.5 %) in the Gleysol A1 horizon. The accumulation of calcium carbonate was mainly characteristic in the mineral horizons of the soils with shallow groundwater. The particle size distribution of the soils was dominated by the clay and silt fractions except in the Phaeozem, where the dominance of the sand and clay fractions was characteristic. Significant Fe accumulation could not be observed in the bulk soils, exhibiting a slight peak in the subsoil with the highest value (7.45

%) in the Solonetz C horizon. Goethite could only be identified in the bulk soil and clay fractions of certain horizons, and it failed in the Solonetz and Pellic Vertosil profiles.

Ferromanganese nodules appeared in the soils within large depth intervals except in the Gleysol and Pellic Vertisol, where they were restricted to a single horizon. The horizons containing nodules did not show a significant Fe accumulation but exhibited a more clayey texture than the other horizons. Besides ferromanganese nodules, calcareous nodules also appeared in some soil horizons. Large (up to 10 mm), ellipsoid and branch-shaped nodules were found in the Gleysol A2 and B horizons (Fig. S1). Large (up to 10 mm), ellipsoid and irregular nodules, and smaller (up to 5 mm) irregular nodules were observed in the Solonetz BC and C horizons, respectively (Fig. S1). Finally, calcified root cells up to 5 mm in length were found in the Phaeozem *C*2 horizon (Fig. S3). Their XRD analysis showed that they compose primarily of calcite with a subordinate presence of other soil phases, like quartz, feldspar, and clay minerals.

3.2. Nodules characteristics

The major characteristics of the nodules are summarized in Table 2, and their microscopic images are shown in Figures S1, S2, and S3. Three types of nodules could be observed in the studied soils: concentric nodules, concentric nodules with a nucleus, and typic nodules. The latter showed a smaller size, lighter color, and less rounded shape when compared to concentric nodules. All three nodule types appeared in soils formed under different hydromorphic conditions, and they could be present even within the same soil horizon.

The largest nodules (up to 10 mm) were observed in soils with shallow groundwater (Fig. 1). In these soils, typic nodules appeared separately in the deeper soil horizons, and they were even lacking in the soil containing the largest concentric nodules (Gleysol). In the Vertisol and Solonetz profiles, the concentric nodules often had a typic nucleus, although concentric nodules also appeared in the Solonetz profile subordinately. The concentric nodules of these soils generally contained a large number of concentric bands. Nodules closer to the surface were porous, whereas those found in the deeper soil horizons were rather compacted.

Typic nodules were present in each horizon of the soils with stagnant surface water (Fig. 2). Concentric nodules were restricted to certain soil horizons, and they were present in the deeper soil horizons of the Luvisol profile. The nodules of these soils were smaller than those found in the soils with shallow groundwater. The inner structure of their concentric nodules was less developed, e.g., a lower number of concentric bands and a more porous structure were characteristic of them. These features mainly were characteristic also of the soil with regular flooding (Fig. 3). In the Phaeozem profile, concentric nodules with and without a nucleus were present, but the latter type was only present in the deepest soil horizon.

The iron concentration in the nodules was the highest (above 20 %) in the soils with shallow groundwater, primarily where the large concentric nodules were observed. The typic nodules of these soils contained significantly lower Fe amounts, similarly to nodules found in soils with stagnant surface water and regular flooding (between 10 and 15 %). Accordingly, the nodules' Fe content was 5–10-times higher than that of the bulk soils in the former profiles, whereas the enrichment was only 2–3-times higher in the latter ones. Moreover, the concentric nodules of the Vertisol and Gleysol profiles contained a very high amount of goethite (up to 40 %), which recovered 70–90 % of the nodules' Fe content. Such a high recovery ratio was also found in the Vertisol B horizon, where typic nodules appeared only. Much lower recovery ratios were found in the Solonetz profile (between 15 and 25 %) due to the nodules' lower goethite content. However, both in the Vertisol and Solonetz profiles, the nodules' goethite content and the recovery ratio increased upwards. In the soils with stagnant surface water and regular flooding, goethite was detected only in nodule separates where both concentric and typic nodules were present. The goethite Fe recovery ratio was between 15 and 30 % in the Pellic Vertisol and Phaeozem profiles, whereas it was 90 % in the Luvisol *C*2 horizon. The other mineral components of the nodules are similar to those found in the bulk soils, like quartz (30–70 %), feldspars (3–20 %), and clay minerals (6–50 %). A large amount of calcite (15 % and 11 %) was found in the nodules of the GleysolA2 and Solonetz B1 horizons, respectively.

Table 2
The major properties of the ferromanganese nodules found in the studied soils. r = reddish, l = light; n.d. = not detected.

	Type	Size	Shape	Color	Fe %	Fe_{nod}/Fe_{soil}	Goethite %
Soils with shallow groundwater							
VERTISOL							
A	concentric with nucleus	< 5 mm	rounded	r. brown, black, grey	25.87	5.9	29
AB	concentric with nucleus	< 5 mm	rounded	r. brown, grey	22.30	4.5	25
B	typic	< 2 mm	s. rounded, rectangular	l. brown, grey, black	13.54	2.5	15
GLEYSOL							
A2	concentric	< 10 mm	rounded	grey, l. brown, r. brown	28.05	9.2	41
SOLONETZ							
B1	concentric with nucleus	< 2 (5) mm	rounded	r. brown	36.74	9.0	14
B2	concentric with nucleus, concentric	< 5 mm	rounded	black, r. brown	31.64	6.7	7
BC	typic, coated typic	< 5 mm	s. rounded, rectangular	black, r. brown	11.28	2.4	3
Soils with stagnant surface water							
Pellic VERTISOL							
A2	concentric, typic	1 mm	rounded, s. rounded, rectangular	black	11.27	2.8	5
LUVISOL							
C1	typic	< 2 (5) mm	rounded, s. rounded	l. brown, r. brown, black	13.15	2.9	n.d.
*C*2	typic, concentric	< 5 mm	rounded, s. rounded	l. brown, r. brown, black	9.98	2.1	15
Soils with regular flooding							
PHAEOZEM							
A2	concentric with nucleus, typic	< 1 mm	rounded, s. rounded	l. brown, r. brown, grey, black	14.59	3.2	4
B	concentric with nucleus, typic	< 3 mm	rounded	r. brown, black, l. brown	14.18	2.5	n.d.
C1	typic	< 3 mm	rounded, s. rounded, rectangular	l. brown, grey, r. brown, black	11.20	1.9	n.d.
*C*2	typic, concentric	< 3 mm	s. rounded, rectangular	r. brown, black, grey	8.29	1.4	3

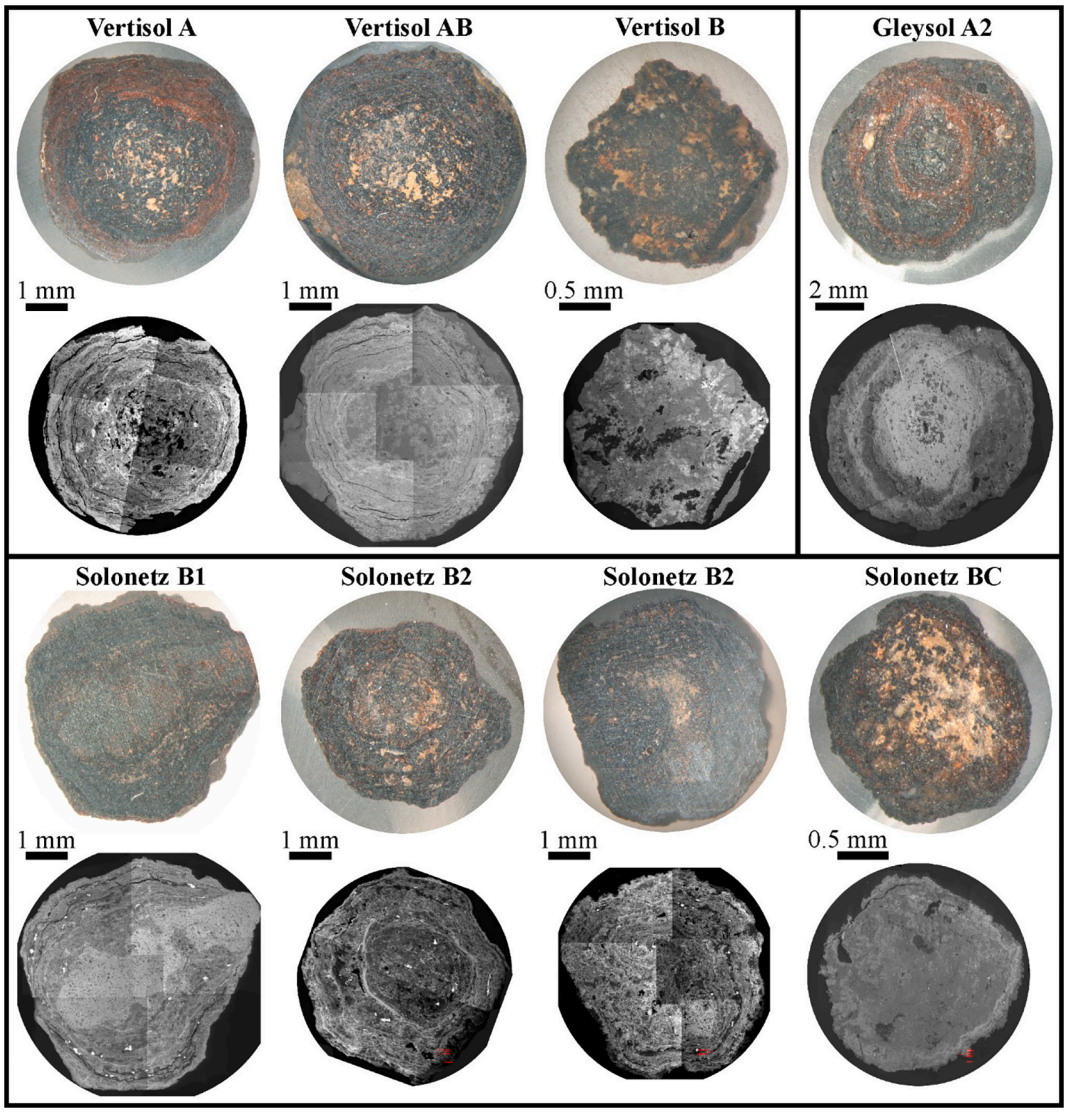

Fig. 1. Stereomicroscopic and backscattered electron images of the characteristic nodule types found in the different horizons of the soils with shallow groundwater.

3.3. Iron isotope characteristics of soils and nodules

The Fe isotopic compositions of the studied soil profiles and nodules are shown in Table 3 and illustrated in Fig. 4. The δ ^{56}Fe values of the soils were between −0.24 and + 0.12 ‰, whereas between −1.16 and −0.26 ‰ for the nodules. The nodules exhibited more negative values than the corresponding soils. The difference between the δ ^{56}Fe values of the soils and nodules decreased in the order of Pellic Vertisol, Vertisol, Solonetz, Phaeozem, Luvisol, and Gleysol, from 1.24 to 0.23 ‰. Among the soils with shallow groundwater, the Vertisol profile exhibited δ ^{56}Fe values close to 0.0 ‰ with a slight minimum in the horizon B (-0.06 ‰). In the nodules, however, this value showed a slight increase with depth from −0.81 to −0.54 ‰. Similar profile distribution was found in the Gleysol with a minimum of −0.11 ‰ in the B horizon, whereas the δ ^{56}Fe value was −0.37 ‰ for the nodules. The Solonetz profile showed slightly negative δ ^{56}Fe values (between −0.15 and −0.20 ‰) with two maxima around 0.0 ‰ in the B1 and BC horizons. In the nodules, very similar values were found between −0.65 and −0.75 ‰.

Among the soils with stagnant surface water, the δ ^{56}Fe values showed a uniform distribution around 0.0 ‰ in the Pellic Vertisol, and the nodules showed a much lower value of −1.16 ‰. Similarly, δ ^{56}Fe values around 0.0 ‰ were characteristic of the Luvisol profile with slight positive maxima of + 0.09 and + 0.07 ‰ in the B and *C*2 horizons, respectively. The δ ^{56}Fe values of the nodules were less negative at lower soil depths (-0.43 and −0.24 ‰) in this profile. The Phaeozem characterized by regular flooding also exhibited δ ^{56}Fe values around 0.0 ‰ with slightly positive (between + 0.06 and + 0.11 ‰) and negative (-0.23 ‰) values of the upper and lower horizons, respectively. In the nodules, less negative values were found again in the lower soil depth (between −0.66 and −0.46 ‰).

The total Fe concentrations and the δ δ ^{56}Fe values of the bulk soils exhibited a reverse pattern with depth in the most studied profiles, except for the Pellic Vertisol. The phenomenon was also characteristic in the relation of the nodules' total Fe concentration and δ ^{56}Fe values (Fig. 4).

4. Discussion

4.1. Nodules development related to the hydromorphic conditions

Similar nodule types were found in the soils formed under different hydromorphic conditions, and their vertical distribution also showed similarities. The nodule types and their spatial distribution characteristics are visualized in Fig. 5. Large concentric nodules have developed in the most intense groundwater fluctuation zone. These nodules are generally compacted and can be characterized by many concentric

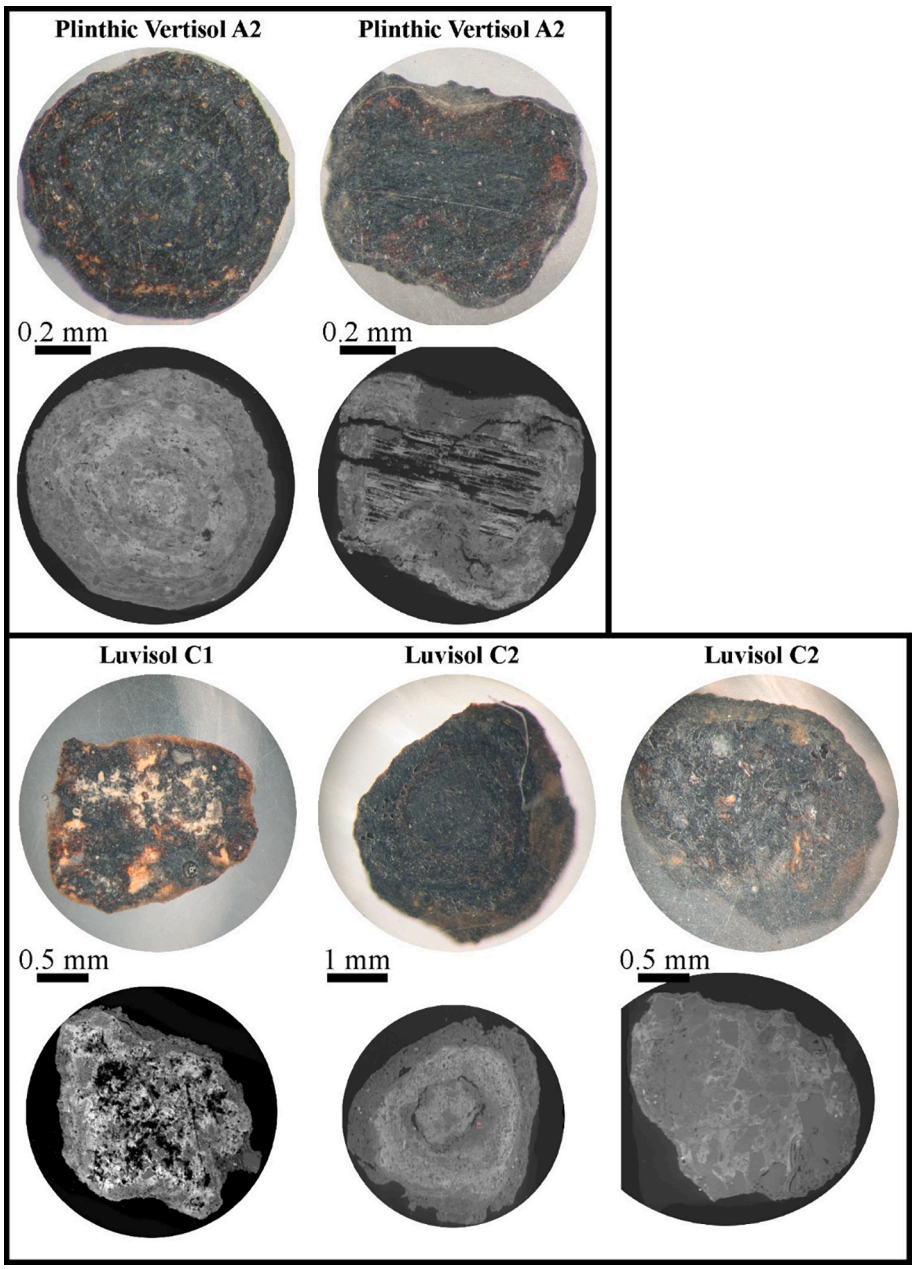

Fig. 2. Stereomicroscopic and backscattered electron images of the characteristic nodule types found in the different horizons of the soils with stagnant surface water.

bands, high iron accumulation, and a high ratio of crystalline Fe-oxyhydroxides. Concentric nodules may also form above this zone, with smaller size, lower frequency, and higher porosity. The smaller typic nodules are rather characteristic of the deeper soil horizons under frequent saturation. Their porosity can be as low as the concentric ones formed above them, but the rate of iron accumulation and that of the crystalline Fe-oxyhydroxides are generally lower. In certain cases, typic nodules can occasionally be coated by a (few) concentric bands showing Eh fluctuation at lower soil depths. Such nodule types were observed in most hydromorphic soils (Palumbo et al., 2001; Timofeeva et al., 2014, Gasparatos et al., 2019). Earlier studies also showed that nodules often vary in frequency, size, chemistry, and fabric among the different soil horizons, which can be related to different pedogenic stages (Sun et al., 2018). While the banded structure of the nodules formed in response to periodic Eh fluctuation as an accretionary process, shortening the periods of oxidation and/or reduction may result in the development of nodules with a lower number of bands or even that of the typic nodules (Gasparatos et al., 2019). In laboratory experiments, Thompson et al. (2006) found that redox oscillations may increase the crystallinity of Fe-oxyhydroxides. During the nodule development, crystalline Fe-oxyhydroxides may enrich through residual enrichment when subsequent mineral dissolution and recrystallization occur. On the contrary, several factors in the soil inhibit the development of the nodules' structure. Jien et al. (2010) observed that smaller-sized nodules were formed in soil horizons with higher organic matter content. Even small amounts of organic matter could affect the ferrihydrite's particle size and structural order (Eusterhues et al., 2008), and the low crystalline Fe-oxyhydroxides are more prone to dissolution when compared to the crystalline ones (Bonneville et al., 2009). All these conditions may favor the formation of less developed concentric nodules above the zone of the most intense water fluctuation. In contrast, extended reduction periods may inhibit the development of concentric bands around the nodules

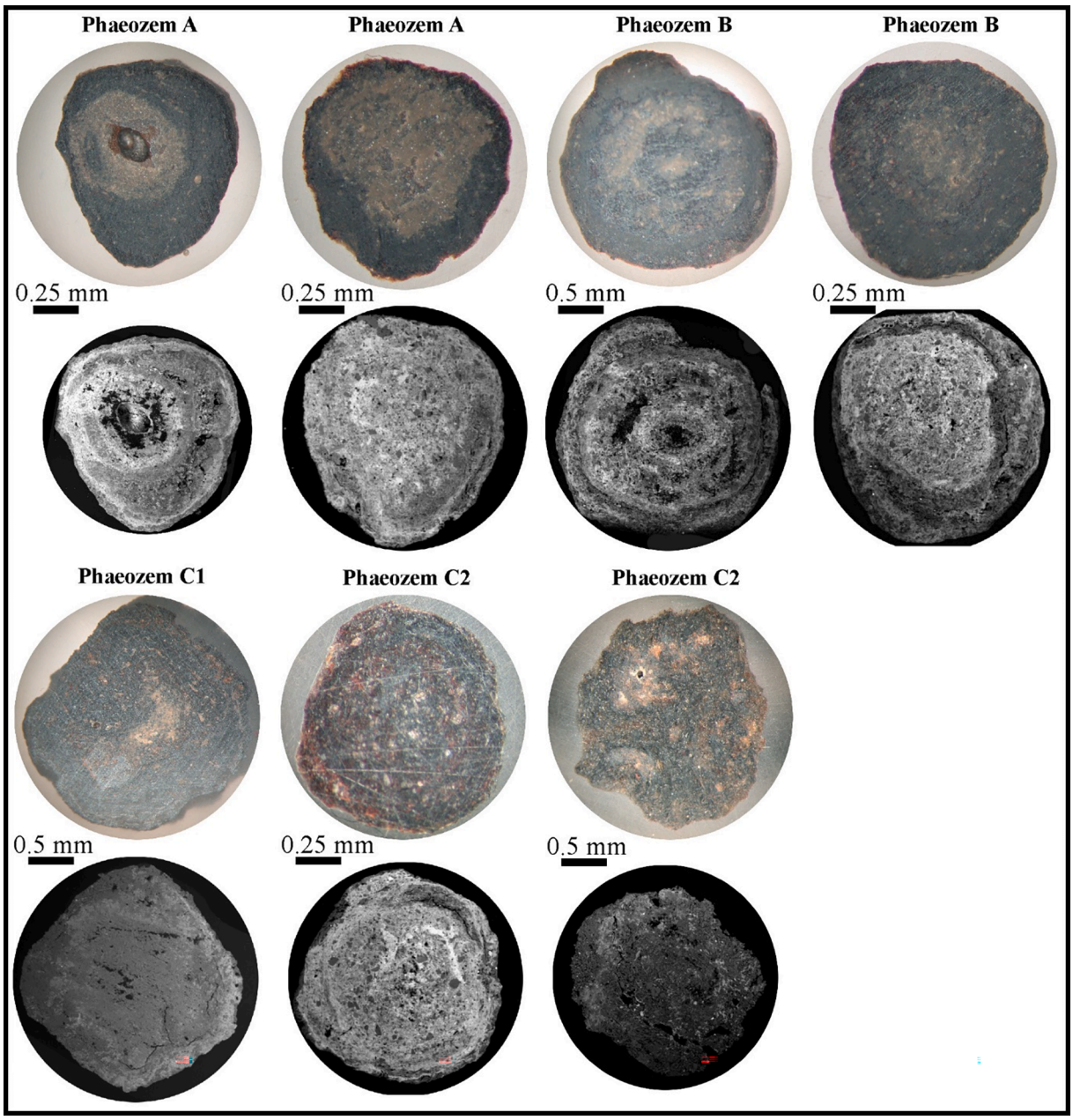

Fig. 3. Stereomicroscopic and backscattered electron images of the characteristic nodule types found in the different horizons of the soil with regular flooding.

due to the dissolution of Fe-oxyhydroxides. However, the oxidization potential of the nodules inhibits their complete dissolution (Sun et al., 2018), resulting in the formation of typic nodules below the zone of water level fluctuation.

The nodules contained calcite in the Gleysol A2 and Solonetz B1 horizons. Others (Sanz et al., 1996; Segvic et al., 2018; Gao et al., 2018) also identified calcite in the ferromanganese nodules. Carbonate nodules appeared in the subsoil of both profiles (Fig. S1) suggesting their formation through downward leaching and precipitation. However, groundwater fluctuation may have resulted in both upward movement and re-precipitation, and in-situ formation of carbonates, as well (Zamanian et al., 2016). Authigenic calcite precipitations were observed within the nodules of the Gleysol directly by Sipos et al. (2022). Although it failed for the nodules of the Solonetz profile, the sub-microscopic size of the calcite suggests in situ formation in those nodules, too. The precipitation of calcite and ferrihydrite probably did not proceed simultaneously in the nodules; rather they provided an appropriate surface for each other to precipitate under the influence of a neutral-alkaline environment and redox fluctuations. For example, Yoshida et al. (2018) interpreted the formation of Fe-oxide concretions through the transformation of carbonate precursors via pH-buffering. Contrarily, carbonate ions form inner-sphere complexes on the ferrihydrite surface, and the presence of carbonate may even enhance ferrihydrite dissolution at alkaline pH through the formation of Fe(III)–CO_3 complexes (Mendez and Hiemstra, 2019), promoting the goethite formation through dissolution-crystallization processes (Cudennec and Lecerf, 2006). Such processes may have also contributed to the relatively high goethite content of the nodules of the Gleysol profile. However, the lack of calcite in the bulk soil of the B1 horizon of the Solonetz profile, and its near-neutral pH suggest that the inclusion of calcite within the nodules impeded the leaching of carbonate completely from this horizon. However, further investigations are needed to explain the paragenetic relationship between the carbonate and Fe-oxyhydroxide phases in the nodules in more detail.

Table 3
The Fe isotope characteristics of the studied soils and nodules.

	Soil		Nodule		Soil		Nodule	
	δ56Fe	stdev	δ56Fe	stdev	δ57Fe	stdev	δ57Fe	stdev
Soils with shallow groundwater								
VERTISOL								
A	0.071	0.051	−0.814	0.057	0.081	0.100	−1.185	0.108
AB	−0.017	0.115	−0.761	0.063	0.001	0.224	−1.099	0.104
B	−0.058	0.091	−0.538	0.065	−0.087	0.118	−0.876	0.211
C	0.121	0.108			0.180	0.131		
GLEYSOL								
A1	0.063	0.060			0.106	0.113		
A2	−0.044	0.054	−0.370	0.120	−0.045	0.077	−0.524	0.219
B	−0.105	0.085			−0.132	0.099		
C	0.064	0.086			0.101	0.149		
SOLONETZ								
A	−0.145	0.151			−0.208	0.250		
B1	0.040	0.074	−0.651	0.168	0.063	0.106	−0.930	0.311
B2	−0.186	0.135	−0.705	0.091	−0.290	0.221	−1.043	0.157
BC	−0.041	0.125	−0.745	0.253	−0.062	0.184	−1.031	0.345
C	−0.237	0.178			−0.343	0.272		
Soils with stagnant surface water								
Pellic VERTISOL								
A1	−0.029	0.026			−0.018	0.058		
A2	0.080	0.152	−1.156	0.053	0.134	0.256	−1.680	0.057
AB	0.036	0.055			0.045	0.097		
LUVISOL								
A	0.008	0.056			0.026	0.056		
B	0.094	0.054			0.158	0.101		
C1	−0.011	0.050	−0.434	0.051	−0.086	0.210	−0.622	0.052
C2	0.068	0.052	−0.242	0.145	0.072	0.087	−0.341	0.246
C3	−0.019	0.060			−0.003	0.102		
Soils with regular flooding								
PHAEOZEM								
A1	0.060	0.128			0.125	0.123		
A2	0.118	0.046	−0.658	0.053	0.176	0.083	−1.110	0.140
B	0.005	0.056	−0.597	0.178	0.150	0.368	−0.862	0.279
C1	0.009	0.054	−0.496	0.088	0.013	0.084	−0.734	0.138
C2	−0.232	0.167	−0.462	0.049	−0.251	0.263	−0.845	0.199

The vertical distribution of different nodule types described above is the most characteristic of soils with shallow groundwater table. In these soils, large concretions with a high number of concentric bands form exceptionally when the water fluctuation is very intense within a narrow depth interval. Additionally, an external iron source can also be supposed in these cases. In seasonally saturated soils (due to stagnant surface water or flooding), the less intense water fluctuation results in smaller nodule size, higher porosity, lower iron accumulation, and a lower ratio of crystalline Fe-oxyhydroxides. Additionally, concentric and typic nodules may appear within the same horizon in such soils, suggesting the frequent relocation of the water fluctuation zone. Timofeeva et al. (2014) showed that high differentiation in fabric and chemistry and a high ratio of crystalline Fe-oxyhydroxides are characteristic of large-sized nodules. On the contrary, Yu et al. (2020) found that larger nodules do not necessarily have a more developed band structure. We also found that concentric nodules may be even characterized by a low ratio of crystalline Fe-oxyhydroxides. Yu and Lu (2016) explained this phenomenon through the rapid changes in the soil Eh. All these results suggest that more extended redox periods are necessary for the crystallization of Fe-oxyhydroxides than for the development of the concentric structure. According to Vogelsang et al. (2016), the trend of increasing portions of less crystalline goethite in paddy soils can be explained by either insufficient time for recrystallization of ferric precipitates or the decrease in crystal size of Fe-oxyhydroxides present upon partial reductive dissolution. Although concentric nodules do not necessarily contain a high ratio of crystalline Fe-oxyhydroxides, the duration of waterlogging plays a significant role in the nodule formation, besides the intensity of water oscillation. Chen et al. (2019) also found differences in (hydrous) Fe-oxide crystallinity within redoximorphic soils. They also explained it by the different timescale of Fe redox cycling or differences in processes affecting the crystallization of these phases.

The appearance of concentric nodules with a nucleus can also be due to the relocation of the water fluctuation zone. These nodules developed as typic nodules first, but a series of concentric bands coat them after the relocation of the water fluctuation zone into the horizon where they have been formed. This process is the most characteristic of soils with regular flooding. Another explanation is the change in the water fluctuation rate within the given soil horizon, which is characteristic of soils with stagnant surface water or shallow groundwater. Concentric nodules with a nucleus were observed in several studies (e.g., Stiles et al., 2001; Pai et al., 2003). Sun et al. (2018) considered this process the first stage of the formation of a well-developed nodule. The formation rate of the nodules is controlled by the changes in the frequency of the redox potential of the soil (Yu et al., 2020). The concentric bands formed due to the rapidly changing Eh could be characterized by larger porosity and relatively lower contents of Fe and Mn. In contrast, the reverse was true for the concentric bands formed due to the slowly changing redox potential. Thus, relocation of the groundwater fluctuation zone in the soil may result in the appearance of nodules being at a different stage of their development even within a single horizon.

4.2. Iron isotope fractionation during the formation of nodules

The δ ^{56}Fe values showed nearly uniform distribution with depth in the studied soils, although slight variances could be observed in most

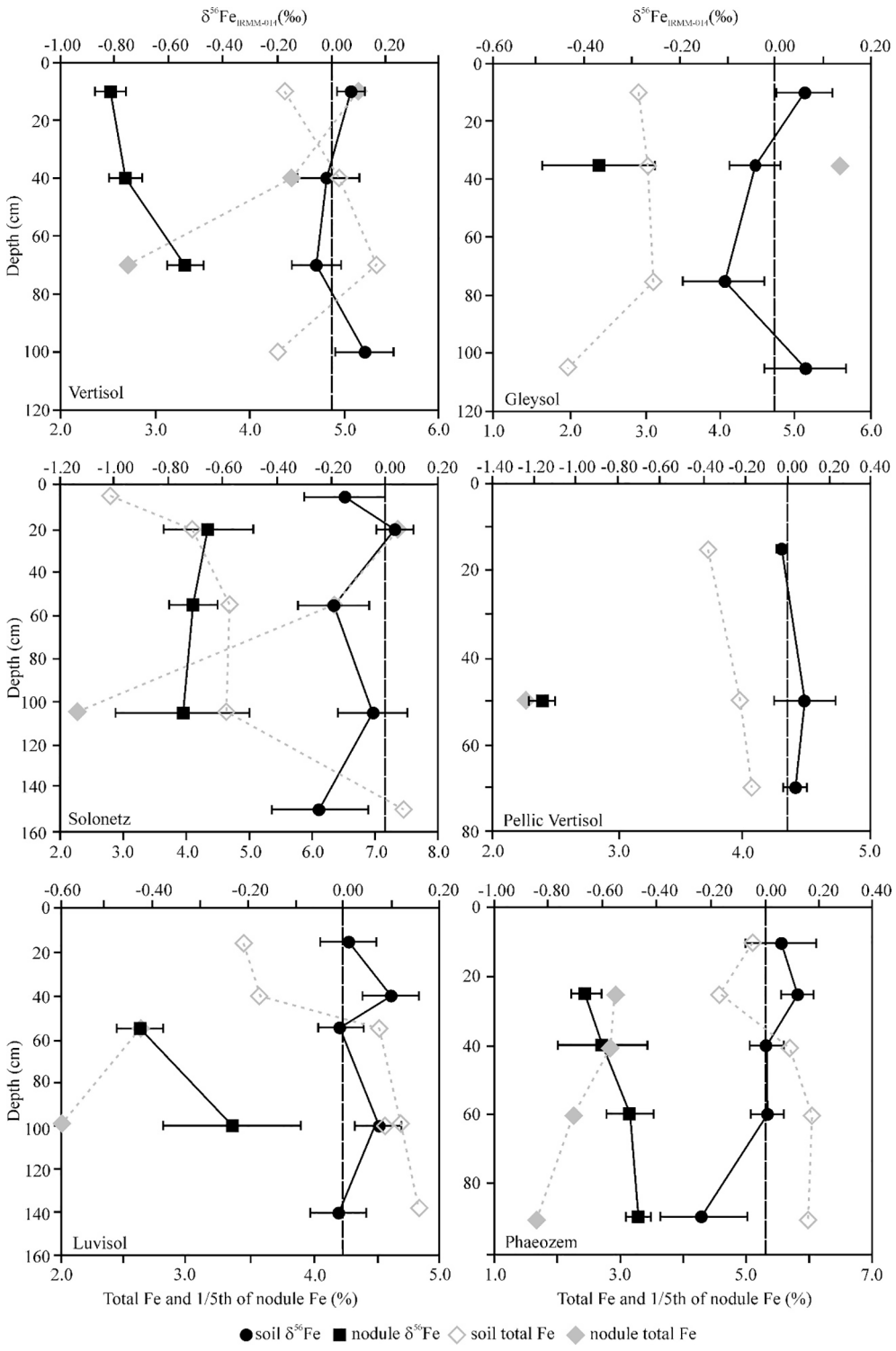

Fig. 4. Distribution of δ ^{56}Fe values and total Fe concentrations within the studied soil profiles and nodules. Black circles and squares represent δ ^{56}Fe values for soils and nodules, whereas open and grey diamonds represent Fe concentrations for soils and nodules, respectively.

cases. Such distribution was found in several soil types, even in hydromorphic ones, despite the large variety of their total Fe content. The phenomenon was explained by the limited spatial transport of Fe within the profile (Wiederhold et al., 2007), the masking effect by the isotope signature of the bulk soil (Huang et al., 2018), or the selective removal of isotopically fractionated Fe in the soil (Lotfi-Kalahroodi et al., 2021). Additionally, the presence of an external Fe source may also contribute to the isotopic signal of the bulk soil (Feng et al., 2018; Huang et al., 2018), primarily for soils with shallow groundwater from groundwater upwelling or higher topographic positions, which all transport isotopically light Fe into the soil (Schuth et al., 2015). Thus, the Fe isotope composition of a specific soil horizon results from a complex interaction of different processes.

Generally, the preferential release of isotopically light Fe is expected under reductive dissolution (Wu et al., 2019). In our case, it was indicated by the reverse vertical distribution pattern of the δ ^{56}Fe values and

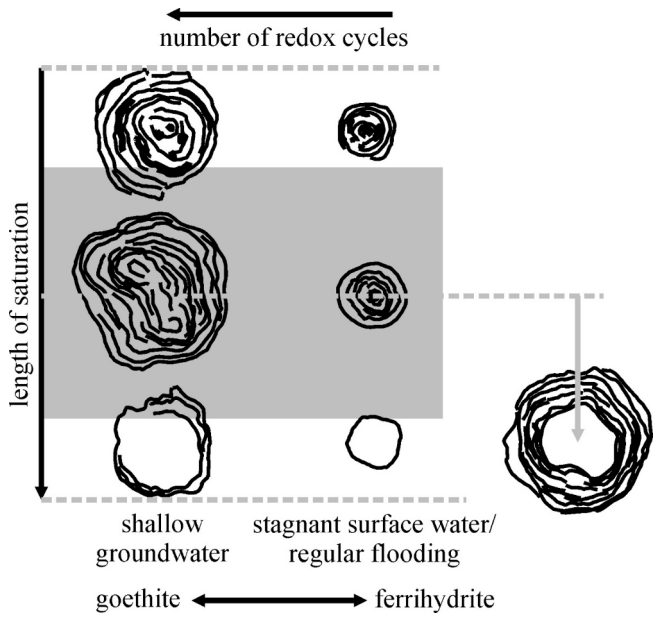

Fig. 5. Major nodule types and their spatial distribution characteristics under different hydromorphic conditions.

total Fe concentrations of the bulk soils and nodules on the one hand. This shows the preferential loss of lighter Fe isotopes in the Fe-depleted zones of the profiles. The phenomenon was also observed by Huang et al. (2018) in a paddy soil chronosequence. They suggested that simultaneous plant uptake and reductive dissolution of Fe-minerals result in the gradual depletion of light Fe isotopes in the topsoil. Meanwhile, the dissolved light Fe precipitates in the Fe enrichment zone of the subsoil. Groundwater fluctuation may induce a re-dissolution and transport of Fe from the enrichment zones, creating further enrichment and depletion zones in the subsoil. In a long timescale, light Fe isotopes could be leached out of the pedon causing the enrichment of heavy Fe isotopes in the residual soil. In our case, the vertical distribution pattern of total Fe concentration and δ^{56}Fe values could be corresponded to those found in the paddy soils by Huang et al. (2018) at different cultivation ages. The Pellic Vertisol exhibited similar characteristics to the young paddy soils. The Luvisol and Solonetz profiles showed similarities to the paddy soils of transitional cultivation ages, whereas the Vertisol, Gleysol, and Phaeozem profiles to the aged paddy soils. In our case, however, not (only) the age of the soil but the frequency and rate of the redox cycles were primarily responsible for the vertical distribution pattern of total Fe concentration and δ^{56}Fe values.

On the other hand, the preferential release of the isotopically light Fe was also indicated by the lighter Fe isotopic composition of the nodules than the bulk soils. This phenomenon was also found by Feng et al. (2018) for paleo-concretions in terra rossa soil. Additionally, similar features were also observed in redoximorphic soils when the isotopic compositions of Fe-enriched and depleted zones were compared (Schulz et al., 2016; Huang et al., 2018; Fekiacova et al., 2021). Processes resulting in the formation of nodules, like dissolution, reduction, adsorption, and precipitation, all could result in Fe isotopic fractionation at varying degrees (Brantley et al., 2004; Teutsch et al., 2005; Clayton et al., 2005; Chapman et al., 2009). Due to their initial formation as pore fillings (Yu et al., 2020), the Fe of the nodules is composed of Fe from the soil matrix and the newly formed Fe-oxyhydroxides (Feng et al., 2018). Consequently, the isotopic characteristics of the nodules also support that authigenic Fe-oxyhydroxides in soils enrich the light Fe isotope. When nodules appeared in several horizons within a profile, their isotopic composition shifted towards less negative values downwards despite the more negative δ^{56}Fe values for the bulk soils. The extended reductive periods in the subsoil resulted in the partial re-dissolution of the nodules' Fe-oxyhydroxides. Thus, isotopically light Fe left the nodules preferentially. This phenomenon was not only characteristic of soil nodules with a large ratio of non-crystalline Fe-oxyhydroxides but also of those containing a higher ratio of goethite. According to Schuth and Mansfeldt (2016), the combined adsorption and atom exchange between dissolved Fe and Fe-oxyhydroxides affects the isotopic composition of the latter ones. They found that the soil solution in the Fe-rich horizons of Gleysols exhibited significantly lower δ^{56}Fe values than in Fe-poor horizons. Although non-crystalline Fe-oxyhydroxides are more prone to dissolution, the goethite content of the nodules did not recover the total Fe content of the nodules in any case either. Thus, nodules of each studied soil contained a certain amount of non-crystalline Fe-oxyhydroxides, which could be dissolved under reductive conditions. At high reduction rates, Fe(II) in solution is significantly lighter in isotope composition than ferrihydrite, reflecting a kinetic fractionation effect. This effect could be related to dissolution but also the fast sorption of Fe (II) on the ferrihydrite surface (Wu et al., 2019).

The minimum δ^{56}Fe values were found below the most intense water fluctuation zone in the Vertisol, Gleysol, and Phaeozem profiles. Thus, the minimum δ^{56}Fe value does not reflect the zone of the most frequent groundwater oscillation but the deepest part of the soil where precipitation of light Fe may dominate over its leaching. The downward transportation of the light Fe isotopes within the whole depth interval of the water fluctuation zone was also observed in hydromorphic soils (e.g., Wiederhold et al., 2007; Mansfeldt et al., 2012; Qi et al., 2020). The net result of open-system Fe cycling favors the removal of light Fe from the soil profile when total Fe loss is dominated by reductive dissolution (Thompson et al., 2007). Fekiacova et al. (2013) found that the behavior of the oxide-bound Fe dominates the Fe isotopic composition of such soils. As long as reductive conditions are not prevailing, the isotopically light Fe may be precipitated to form the nodules. In contrast, its leaching is characteristic of the C horizons, as indicated by their slightly positive δ^{56}Fe values in our case. Qi et al. (2020) also observed similar Fe isotopic features in horizons under reducing conditions in paddy soils. In the Phaeozem, however, the zone of dominant reductive conditions was not reached, probably due to the much broader depth interval and the seasonal presence of water fluctuation in the soils with regular flooding. Thus, enrichment in heavy Fe isotopes of the deepest soil horizons could not be observed in this case.

The difference between the δ^{56}Fe values of the bulk soils and nodules decreased downwards both in the Vertisol and Phaeozem despite the large differences in the nodules' properties in the two soils. This difference suggests that the Fe isotope fractionation, the nodules' development, and the Fe-oxyhydroxides' crystallization are carried out at different time scales. However, the stable supply of Fe in solution may result in very similar isotopic characteristics for soils with nodules having significantly different properties. As the ratio of the non-crystalline Fe-oxyhydroxides in the nodules did not change with depth, the higher frequency of the reductive conditions was responsible primarily for the higher mobilization of isotopically light Fe from the nodules in the lower soil horizons. On the contrary, a relatively small difference was observed between the bulk soil and nodule δ^{56}Fe values in the Gleysol despite the large, well-developed concretions with a very high ratio of goethite. Besides the downward leaching of isotopically light Fe, the very intense redox oscillation may have promoted the more intense re-dissolution of isotopically light Fe from the nodules' Fe-oxyhydroxides in this soil. According to Schuth et al. (2015), the breakdown of (hydrous) Fe-oxides under weakly reducing conditions will already result in a preferential removal of light Fe and an increase of heavy Fe of the remaining solid phase with time, even at moderate Eh values but still above the Eh limit of Fe(III) reduction.

The oscillating distribution of the δ^{56}Fe values in the Solonetz and Luvisol profiles suggests that the leaching of isotopically light Fe is more characteristic of certain horizons than others. These two soils are the deepest profiles among the studied ones, and the occasional relocation of the water fluctuation zone could be a more frequent phenomenon.

This may result in the varying intensity of leaching among the soil horizons. According to Fekiacova et al. (2013), groundwater level fluctuations could induce the translocation of isotopically fractionated Fe after the dissolution of their oxides. And the solubilized Fe may then be translocated downwards by leaching and upwards by capillary rise. Feng et al. (2018) also explained the fluctuation of the δ ^{56}Fe values by the systematic changes in redox conditions within a terra rossa profile containing nodules. The frequent relocation of the water fluctuation zone may have also promoted the homogeneous isotopic composition of the nodules with depth in the Solonetz profile despite the decreasing content of Fe and crystalline Fe-oxyhydroxides in the nodules with depth. Contrarily, the less negative δ ^{56}Fe values of the nodules in the deeper horizon of the Luvisol can still be related to the higher rate of redissolution due to the higher frequency of reductive conditions.

As long as δ ^{56}Fe did not exceed 0.0 ‰ significantly in the Solonetz, it often exhibited positive values in the Luvisol. The difference may be related even to the differences in hydromorphic conditions of the two soils. The Luvisol with stagnant surface water represents a relatively closed system, where the mobilization of isotopically light Fe results in a local maximum of the bulk δ ^{56}Fe values. In contrast, its precipitation is restricted to the nodules without being leached out of the soil. However, in the Solonetz profile located at a low topographic position (Novák and Tóth, 2016), isotopically light Fe may enter the profile from soils at higher topographic positions. The supply of isotopically lighter Fe from higher topographic positions may induce an isotopic rejuvenation in soils. The rejuvenation means that light Fe was leached due to redox processes to lower topographic positions resulting in a lack of enrichment of such soils in heavy Fe isotopes (Akerman et al., 2021).

In the Pellic Vertisol, the nodule formation is restricted to a very narrow soil depth interval. In this soil, the relatively fast and local precipitation of the isotopically light Fe within the nodules can be supposed. The lack of leaching is also supported by the largest difference between the δ ^{56}Fe values of the nodules and the bulk soil among the studied profiles. Kinetic effects also favor light Fe isotopes during rapid precipitation of Fe-oxyhydroxides in soils where the reactive dissolved iron pool is continuously separated from the precipitate (Garnier et al., 2017). Kiczka et al. (2011) showed that kinetic fractionation effects might persist during long-term weathering in field systems and dominate Fe isotope fractionation in young weathering environments. Redox processes may result in a significant Fe isotope fractionation within a soil horizon, even in soil profiles where no Fe isotope fractionation could be observed with depth. The flux of light Fe must be low in such cases, and it does not significantly influence the isotopic signature of the bulk soil (Fekiacova et al., 2021). Mass balance considerations also suggested that the isotope signature of a large pool (e.g., soil minerals) changes much less than a small pool (e.g., soil solution) during the fractionation reaction. As dissolution reactions occur predominantly at mineral surfaces, the isotope signature of the depleted residue changes only along this reaction front (Wiederhold et al., 2007).

5. Conclusions

Differences among hydromorphic conditions may result in both similar and different properties of the ferromanganese nodules formed in the soil. The extent of hydromorphism can be strongly related to the nodules' properties, but such a relationship could not be observed with their Fe isotopic characteristics. The stable supply of Fe in solution due to the reductive dissolution of primary Fe minerals may result in very similar isotopic characteristics for soils with nodules having significantly different properties. However, specific features of hydromorphic conditions may affect the Fe isotope characteristics of both bulk soils and nodules. These characteristics are the frequency and rate of redox cycles, frequent relocation of the water fluctuation zone, topographic positions allowing the external Fe input in soils with shallow groundwater, and inhibition of Fe leaching out of the soils with stagnant surface water.

The nodules' development, the Fe-oxyhydroxides' crystallization, and the Fe isotope fractionation are carried out at different timescales. The minimum δ ^{56}Fe value does not reflect the zone of most frequent groundwater oscillation but the deepest part of the soil where precipitation of light Fe may dominate over its leaching. As long as reductive conditions are not prevailing, the isotopically light Fe may be precipitated to form the nodules. On the contrary, the higher frequency of the reductive conditions is responsible for the higher mobilization of isotopically light Fe from the soil in the subsoil horizons. The isotopic characteristics of the nodules supported that authigenic Fe-oxyhydroxides in hydromorphic soils are enriched in the light Fe isotope.

The Fe isotope composition of a given soil horizon and its nodules result from a complex interaction of different processes whose effect varies from profile to profile. The integrated study of the Fe isotope characteristics of hydromorphic soils and their nodules may help follow pedogenic processes and conditions, like precipitation, leaching, redissolution, external Fe sources, and inhibited leaching. The results of such studies on recently active systems can be even used to differentiate the contribution of certain pedogenic processes even in paleo soil systems and to the overall Fe cycle. Furthermore, an interesting question is the effect of seasonal variation of water saturation on the Fe isotopic properties of hydromorphic soils and ferromanganese nodules found in them.

Declaration of Competing Interest

The authors declare that they have no known competing financial interests or personal relationships that could have appeared to influence the work reported in this paper.

Data availability

Data will be made available on request.

Acknowledgments

This study was supported by the European Union and the State of Hungary and co-financed by the European Regional Development Fund (GINOP-2.3.2-15-2016-00009 "ICER"), and by the Hungarian National Research, Development and Innovation Office (K 119475).

Appendix A. Supplementary data

Supplementary data to this article can be found online at https://doi.org/10.1016/j.geoderma.2022.116286.

References

Akerman, A., Oliva, P., Poitrasson, F., Boaventura, G.R., da Silva Souza, V., Seyler, P., 2021. Impact of deforestation on soil iron chemistry and isotope signatures in Amazonia. Chem. Geol. 577, 120048 https://doi.org/10.1016/j.chemgeo.2020.120048.

Bonneville, S., Behrends, T., Van Cappellen, P., 2009. Solubility and dissimilatory reduction kinetics of iron(III) oxyhydroxides: a linear free energy relationship. Geochim. Cosmochim. Acta 73, 5273–5282. https://doi.org/10.1016/j.gca.2009.06.006.

Brantley, S.L., Liermann, L.J., Guynn, R.L., Anbar, A., Icopini, G.A., Barling, J., 2004. Fe isotopic fractionation during mineral dissolution with and without bacteria. Geochim. Cosmochim. Acta 68, 3189–3204. https://doi.org/10.1016/j.gca.2004.01.023.

Chapman, J.B., Weiss, D.J., Shan, Y., Lemburger, M., 2009. Iron isotope fractionation during leaching of granite and basalt by hydrochloric and oxalic acids. Geochim. Cosmochim. Acta 73, 1312–1324. https://doi.org/10.1016/j.gca.2008.11.037.

Chen, C., Barcellos, D., Richter, D.D., Schroeder, P.A., Thompson, A., 2019. Redoximorphic Bt horizons of the Calhoun CZO exhibit depth-dependent iron-oxide crystallinity. J. Soils Sediments 19, 785–797. https://doi.org/10.1007/s11368-018-2068-2.

Clayton, R., Hudson-Edwards, K., Malinovsky, D., Andersson, P., 2005. Fe isotope fractionation during the precipitation of ferrihydrite and transformation of

ferrihydrite to goethite. Miner. Mag. 69, 667–676. https://doi.org/10.1180/0026461056950278.
Cornell, R.M., Schwertmann, U., 2003. The Iron Oxides: Structure, Properties, Reactions, Occurrences, and Uses. Wiley-VCH Verlag GmbH & Co., KGaA, Weinheim.
Craddock, P.R., Dauphas, N., 2011. Iron isotopic compositions of geological reference materials and chondrites. Geostand. Geoanal. Res. 35, 101–123. https://doi.org/10.1111/j.1751-908X.2010.00085.x.
Cudennec, Y., Lecerf, A., 2006. The transformation of freeihydrite into goethite or hematite, revisited. J. Solid State Chem. 179, 716–722. https://doi.org/10.1016/j.jssc.2005.11.030.
de Jong, J., Schoemann, V., Tison, J.L., Becquevort, S., Masson, F., Lannuzel, D., Petit, J., Chou, L., Weiss, D., Mattielli, N., 2007. Precise measurement of Fe isotopes in marine samples by multi-collector inductively coupled plasma mass spectrometry (MC-ICP-MS). Anal. Chim. Acta 589, 105–119. https://doi.org/10.1016/j.aca.2007.02.055.
Dövényi, Z., 2010. Magyarország kistájainak katasztere. MTA Földrajztudományi Kutatóintézet, Budapest.
Eusterhues, K., Wagner, F.E., Häusler, W., Hanzlik, M., Knicker, H., Totsche, K.-U., Kögel-Knabner, I., Schwertmann, U., 2008. Characterization of ferrihydrite-soil organic matter coprecipitates by X-ray diffraction and Mössbauer spectroscopy. Environ. Sci. Technol. 42, 7891–7897. https://doi.org/10.1021/es800881w.
Fao, 2006. Guidelines for Soil Description. Food and Agriculture Organization of the United Nations, Rome.
FAO, 2014. World reference base for soil resources. International soil classification system for naming soils and creating legends for soil maps. World Soil Resources Reports No. 106. Food and Agriculture Organization of the United Nations, Rome.
Fekiacova, Z., Pichat, S., Cornu, S., Balesdent, J., 2013. Inferences from the vertical distribution of Fe isotopic compositions on pedogenetic processes in soils. Geoderma 209–210, 110–118. https://doi.org/10.1016/j.geoderma.2013.06.007.
Fekiacova, Z., Montagne, D., Duvivier, A., Guilhou, A., Deschamps, P., Cornu, S., 2021. Evolution of Retisol impacted by artificial drainage: What can we learn from stable Fe isotope ratios? Geoderma 384, 114771. https://doi.org/10.1016/j.geoderma.2020.114771.
Feng, J.L., Pei, L.L., Zhu, X., Ju, J.T., Gao, S.-P., 2018. Absolute accumulation and isotope fractionation of Si and Fe during dolomite weathering and terra rossa formation. Chem. Geol. 476, 340–351. https://doi.org/10.1016/j.chemgeo.2017.11.030.
Gao, T., Ke, S., Wang, S.J., Li, F., Liu, C., Lei, J., Liao, C., Wu, F., 2018. Contrasting Mg isotopic compositions between Fe-Mn nodules and surrounding soils: accumulation of light Mg isotopes by Mg-depleted clay minerals and Fe oxides. Geochim. Cosmochim. Acta 237, 205–222. https://doi.org/10.1016/j.gca.2018.06.028.
Garnier, J., Garnier, J.-M., Vieira, C.L., Akerman, A., Chmeleff, J., Ruiz, R.I., Poitrasson, F., 2017. Iron isotope fingerprints of redox and biogeochemical cycling in the soil water-rice plant system of a paddy field. Sci. Total Environ. 574, 1622–1632. https://doi.org/10.1016/j.scitotenv.2016.08.202.
Gasparatos, D., Tarenidis, D., Haidouti, C., Oikonomou, G., 2005. Microscopic structure of soil Fe-Mn nodules: environmental implication. Environ. Chem. Lett. 2, 175–178. https://doi.org/10.1007/s10311-004-0092-5.
Gasparatos, D., Massas, I., Godelistas, A., 2019. Fe-Mn concretions and nodules formation in redoximorphic soils and their role on soil phosphorus dynamics: current knowledge and gaps. Catena 182, 104106. https://doi.org/10.1016/j.catena.2019.104106.
Gee, G.W., Bauder, J.W., 1986. Particle-size analysis. In: Klute, A. (Ed.), Methods of Soil analysis, Part 1, Physical and Mineralogical Methods. SSSA Book Series, No. 1, SSSA, Madison, pp. 383-411. 10.2136/sssabookser5.1.2ed.c15.
Huang, L.M., Jia, X.X., Zhang, G.L., Thompson, A., Huang, F., Shao, M.A., Cheng, L.M., 2018. Variations and controls of iron oxides and isotope compositions during paddy soil evolution over a millennial time scale. Chem. Geol. 476, 340–351. https://doi.org/10.1016/j.chemgeo.2017.11.030.
Jien, S.H., Hseu, Z.Y., Chen, Z.S., 2010. Hydropedological implications of ferromanganiferous nodules in rice-growing plinthitic Ultisols under different moisture regimes. Soil Sci. Soc. Am. J. 74, 880–891. https://doi.org/10.2136/sssaj2009.0020.
Johnson, C.M., Skulan, J.L., Beard, B.L., Sun, H., Nealson, K.H., Braterman, P.S., 2002. Isotopic fractionation between Fe (III) and Fe (II) in aqueous solutions. Earth Planet. Sci. Lett. 195 (1), 141–153. https://doi.org/10.1016/S0012-821X(01)00581-7.
Kaiser, K., Guggenberger, G., 2000. The role of DOM sorption to mineral surfaces in the preservation of organic matter in soils. Org. Geochem. 31, 711–725. https://doi.org/10.1016/S0146-6380(00)00046-2.
Kiczka, M., Wiederhold, J.G., Frommer, J., Voegelin, A., Kraemer, S.M., Bourdon, B., Kretzschmar, R., 2011. Iron speciation and isotope fractionation during silicate weathering and soil formation in an alpine glacier forefield chronosequence. Geochim. Cosmochim. Acta 75, 5559–5573. https://doi.org/10.1016/j.gca.2011.07.008.
Lotfi-Kalahroodi, E., Pierson-Wickmann, A.C., Rouxel, O., Marsac, R., Bouhnik-Le Coz, M., Hanna, K., Davranche, M., 2021. More than redox, biological organic ligands control iron isotope fractionation in the riparian wetland. Sci. Rep. 11, 1933. https://doi.org/10.1038/s4159 8-021-81494 –z.
Mansfeldt, T., Schuth, S., Häusler, W., Wagner, F.E., Kaufhold, S., Overesch, M., 2012. Iron oxide mineralogy and stable iron isotope composition in a Gleysol with petrogleyic properties. J. Soils Sediments 12, 97–114. https://doi.org/10.1007/s11368-011-0402-z.
McLean, E.O., 1982. Soil pH and lime requirement. In: Page, A. L., Miller, R.H., Keeny, D. R. (Eds.), Methods of soil analysis, Part 2, Chemical and Microbiological Properties, SSSA Book Series, No. 2, SSSA, Madison, pp. 199-224. 10.2134/agronmonogr9.2.2ed.c12.
Mendez, J.C., Hiemstra, T., 2019. Carbonate adsorption to ferrihydrite: competitive interaction with phosphate for use in soil systems. ACS Earth Space Chem. 3, 129-141. 10.1021/acsearthspacechem.8b00160.
Nelson, D.W., Sommers, L.E., 1996. Total carbon, organic carbon, and organic matter. In: Sparks, D.L., Page, A.L., Helmke, P.A., Loeppert, R.H., Soltanpour, P.N., Tabatabai, M.A., Johnston, C.T., Summer, M.E. (Eds.), Methods of Soil Analysis, Part 3, Chemical Methods, SSSA Book Series, No. 3, SSSA, Madison, pp. 961-1010. 10.2136/sssabookser5.3.c34.
Nelson, R.E., 1982. Carbonate and gypsum. In: Page, A. L., Miller, R.H., Keeny, D.R. (Eds.), Methods of soil analysis, Part 2, Chemical and Microbiological Properties, SSSA Book Series, No. 2, SSSA, Madison, pp. 181–197. 10.2134/agronmonogr9.2.2ed.c11.
Novák, T.J., Tóth, Cs.A., 2016. Development of erosional microforms and soils on semi-natural and anthropogenic influenced solonetzic grasslands. Geomorphology 254: 121-129. 10.1016/j.geomorph.2015.11.018.
Pai, C.W., Wang, M.K., Chiang, H.C., King, H.B., Hwong, J.L., Hu, H.T., 2003. Formation of iron nodules in a Hapludult of central Taiwan. Can. J. Soil Sci. 83, 167-172. 10.4141/S02-068.
Palumbo, B., Bellance, A., Neri, R., Roe, M.J., 2001. Trace metal partitioning in Fe-Mn nodules from Sicilian soils. Italy. Chem. Geol. 173, 257–269. https://doi.org/10.1016/S0009-2541(00)00284-9.
Qi, Y.H., Cheng, W., Nan, X., Yang, F., Li, J., Li, D.C., Lundstrom, C., Yu, H., Zhang, G.L., Huang, F., 2020. Irons stable isotopes in bulk soil and sequentially extracted fractions trace Fe redox cycling in paddy soils. J. Agric. Food Chem. 68 (31), 8143–8150. https://doi.org/10.1021/acs.jafc.0c02515.
Sanz, A., Garcia-Gonzalez, M.T., Vizcayno, C., Rodriguez, R., 1996. Iron-manganese nodules in a semi-arid environment. Aust. J. Soil Res. 34, 623–634. https://doi.org/10.1071/sr9960623.
Schulz, M., Stonestrom, D., Lawrence, C., Bullen, T., Fitzpatrick, J., Kyker-Snowman, E., Manning, J., Minch, M., 2016. Structured heterogeneity in a marine terrace chronosequence: upland mottling. Vadose Zone J. 15 (2), 1–14. https://doi.org/10.2136/vzj2015.07.0102.
Schuth, S., Hurraß, J., Münker, C., Mansfeldt, T., 2015. Redox-dependent fractionation of iron isotopes in suspensions of a groundwater-influenced soil. Chem. Geol. 392, 74–86. https://doi.org/10.1016/j.chemgeo.2014.11.007.
Schuth, S., Mansfeldt, T., 2016. Iron isotope composition of aqueous phases of a lowland environment. Environ. Chem. 13, 89–101. https://doi.org/10.1071/EN15073.
Segvic, B., Girardclos, S., Zanoni, G., Gonazlez, C.A., Steimer-Herbet, T., Besse, M., 2018. Origin and paleoenvironmental significance of FeeMn nodules in the Holocene perialpine sediments of Geneva Basin, western Switzerland. Appl. Clay Sci. 160, 22–39. https://doi.org/10.1016/j.clay.2018.01.027.
Sipos, P., Kovács, I., Balázs, R., Tóth, A., Barna, G., Makó, A., 2022. Micro-analytical study of the distribution of iron phases in ferromanganese nodules. Geoderma 405, 115445. https://doi.org/10.1016/j.geoderma.2021.115445.
Stiles, C.A., Mora, C.I., Driese, S.G., 2001. Pedogenic iron-manganese nodules in Vertisols: a new proxy for paleoprecipitation? Geology 29, 943–946. https://doi.org/10.1130/0091-7613(2001)029<0943:PIMNIV>2.0.CO;2.
Stoops, G., 2020. Guidelines for analysis and description of soil and regolith thin sections, 2nd edition. American Society of Agronomy, Crop Science Society of America, Soil Science Society of America, and John Wiley & Sons.
Sun, Z.X., Jiang, Y.Y., Wang, Q.B., Owens, P.R., 2018. Fe-Mn nodules in a southern Indiana loess with a fragipan and their soil forming significance. Geoderma 313, 92–111. https://doi.org/10.1016/j.geoderma.2017.10.025.
Teutsch, N., von Gunten, U., Porcelli, D., Cirpka, O.A., Halliday, A.N., 2005. Adsorption as a cause for iron isotope fractionation in reduced groundwater. Geochim. Cosmochim. Acta 69, 4175–4185. https://doi.org/10.1016/j.gca.2005.04.007.
Thompson, A., Chadwick, O.A., Rancourt, D.G., Chorover, J., 2006. Iron-oxide crystallinity increases during soil redox oscillations. Geochim. Cosmochim. Acta 70, 1710–1727. https://doi.org/10.1016/j.gca.2005.12.005.
Thompson, A., Ruiz, J., Chadwick, O.A., Titus, M., Chorover, J., 2007. Rayleigh fractionation of iron isotopes during pedogenesis along a climate sequence of Hawaiian basalt. Chem. Geol. 238, 72–83. https://doi.org/10.1016/j.chemgeo.2006.11.005.
Timofeeva, Y.O., Karabtsov, A.A., Semal', V.A., Burdukovskii, M.L., Bondarchuk, N.V., 2014. Iron-manganese nodules in Udepts: the dependence of the accumulation of trace elements on nodule size. Soil Sci. Soc. Am. J. 78, 767–778. https://doi.org/10.2136/sssaj2013.10.0444.
Újvári, G., Klötzli, U., Hirschinegg, M., Wegner, W., Hippler, D., Kiss, G.I., Palcsu, L., 2021. Rapid decomposition of geological samples by ammonium bifluoride (NH_4HF_2) for combined Hf-Nd-Sr isotope analyses. Rapid Commun. Mass Spectrom. 35, e9081.
Vogelsang, V., Kaiser, K., Wagner, F.E., Jahn, R., Fiedler, S., 2016. Transformation of clay-sized minerals in soils exposed to prolonged regular alternation of redox conditions. Geoderma 278, 40–48. https://doi.org/10.1016/j.geoderma.2016.05.013.
Wiederhold, J.G., Teutsch, N., Kraemer, S.M., Halliday, A.N., Kretzschmar, R., 2007. Iron isotope fractionation during pedogenesis in redoximorphic soils. Soil Sci. Soc. Am. J. 71, 1840–1850. https://doi.org/10.2136/sssaj2006.0379.
Wu, B., Amelung, W., Xing, Y., Bol, R., Berns, A.E., 2019. Iron cycling and isotope fractionation in terrestrial ecosystems. Earth-Sci. Rev. 190, 323–352. https://doi.org/10.1016/j.earscirev.2018.12.012.
Yoshida, H., Hasegawa, H., Katsuta, N., Maruyama, I., Sirono, S., Minami, M., Asahara, Y., Nishimoto, S., Yamaguchi, Y., Ichinnorov, N., Metcalfe, R., 2018. Fe-oxide concretions formed by interacting carbonate and acidic waters on Earth and Mars. Sci. Adv. 4, eaau0872. 10.1126/sciadv.aau0872.

Yu, X., Lu, S., 2016. Micrometer-scale internal structure and element distribution of Fe-Mn nodules in Quaternary red earth of Eastern China. J. Soils Sediments 16, 621–633. https://doi.org/10.1007/s11368-015-1212-5.
Yu, X., Wang, Y., Zhou, G., Peng, G., Brookes, P.C., 2020. Paleoclimatic fingerprints of ferromanganese nodules in subtropical Chinese soils identified by synchrotron radiation-based microprobes. Chem. Geol. 531, 119357 https://doi.org/10.1016/j.chemgeo.2019.119357.
Zamanian, K., Pustovoytov, K., Kuzyakov, Y., 2016. Pedogenic carbonates: forms and formation processes. Earth-Sci. Rev. 157, 1–17. https://doi.org/10.1016/j.earscirev.2016.03.003.